LiBC electronic, vibrational, structural, and low-temperature chemical behavior of a layered material isoelectronic with MgB_2

A. M. Fogg,[1] P. R. Chalker,[2] J. B. Claridge,[1] G. R. Darling,[1] and M. J. Rosseinsky[1]
[1]*Department of Chemistry, The University of Liverpool, Liverpool L69 3BX, United Kingdom*
[2]*Materials Science Division, Department of Engineering, The University of Liverpool, Liverpool, L69 3BX, United Kingdom*
(Received 4 November 2002; revised manuscript received 14 February 2003; published 17 June 2003)

Magnetic susceptibility, Raman spectroscopy, and temperature-dependent structural data are presented on LiBC, which contains hexagonal sheets with strict B-C alternation. Band structure calculations indicate a large band gap. A small temperature-independent paramagnetic susceptibility is observed, while the in-plane stretching modes are at considerably higher frequencies than in superconducting MgB_2. Electronic structure calculations reveal that the B-C in-plane alternation alone is not responsible for the insulating behavior, as the opening of a gap at the Fermi level is driven by details of the layer stacking sequence. The extreme thermal expansion anisotropy observed in LiBC is discussed in the context of the electronic structure. Low-temperature deintercalation of lithium from between the BC layers is possible to afford Li_xBC with $x \leqslant 0.5$, but Raman data indicate that this is due to formation of amorphous graphitelike phases together with LiBC in a biphasic material, consistent with the absence of superconductivity.

DOI: 10.1103/PhysRevB.67.245106 PACS number(s): 71.20.−b, 61.66.Fn, 74.25.Jb, 74.70.Dd

I. INTRODUCTION

The observation of superconductivity at 39 K in the layered diboride MgB_2 (Ref. 1) has stimulated considerable activity aimed at understanding and enhancing T_c. The *AAA* stacking of graphitelike B_2 sheets with Mg in the interlayer space between hexagon centroids is a common metal diboride structure, but extensive substitutional studies have thus far failed to enhance T_c over the initially reported value. Although isoelectronic with graphite, MgB_2 appears to be metallic due to an unusual self-doping mechanism in which the stabilizing effect of the interlayer Mg (via covalent mixing or ionic potential) on the B $2p_\pi$ states in the layer pushes them down in energy to overlap the in-plane σ bonding states and generate holes in these states at the Fermi energy.[2] The strong coupling of these hole carriers with the in-plane B-B stretching modes, despite the absence of a pronounced density of states peak at the Fermi energy and the low $N(E)$ values associated with sp rather than d band metals, is the commonly accepted cause of the high superconducting transition temperature.

LiBC is the closest known analogue of MgB_2: it is isoelectronic and adopts a related structure (Fig. 1) in which the hexagonal graphitelike sheets persist but now contain strict alternation of B and C on the vertices.[3] This alternation is maintained in the layer stacking motif which gives an AB stacking, with B superposed directly on C. Band structure calculations using a range of methods[4,5] indicate the opening of a gap at the Fermi level in a density of states otherwise very similar to MgB_2 due to the observed strict B-C alternation in the planes. However, recent reports indicate that the temperature dependence of the conductivity is very shallow, with only a threefold resistivity increase on cooling from 300 to 4 K, inconsistent with the predicted gap size.[6] The contrasting electronic properties of LiBC will have considerable implications in the search for chemical analogues of MgB_2, and in this paper we combine temperature-dependent property measurements with electronic structure calculations designed to probe the chemical origin of the differences between the two phases. The observation of the control of metallic behavior by the layer stacking sequence couples strikingly with the pronounced difference in thermal expansion anisotropy between the two phases.

The similarities in the overall electronic structure of LiBC and MgB_2 as revealed by band structure calculations have led to recent suggestions that Fermi level spectroscopy by hole-doping LiBC is a viable route to even higher T_c's than found in MgB_2 itself.[4] We have systematically investigated the low-temperature oxidative deintercalation chemistry of LiBC and found that it is indeed possible to remove up to 50% of the lithium using standard soft chemistry techniques. Although classical powder x-ray diffraction methods show that this proceeds with retention of the LiBC structure, no superconductivity is observed. Raman measurements show that this is because the lithium deintercalation produces amorphous graphitelike material rather than an ordered partly intercalated structure.

II. EXPERIMENT

A. Synthesis

LiBC was synthesized according to the method described by Wörle *et al.*[3] In a typical experiment, 0.180 g B, 0.195 g C, and 0.3225 g Li were sealed in a tantalum ampoule under an atmosphere of argon in an arc furnace. The excess lithium is required as a solvent and to compensate for losses during the reaction. The ampoule was heated, under a flow of argon, to 773 K at a rate of 3 K/min. This temperature was maintained for one hour before being increased to 1773 K at a rate of 3 K/min for a further hour. The sample was then cooled to room temperature at a rate of 10 K/min. The loss of lithium from these reactions through the Ta tube at high temperatures and high lithium vapor pressures is well documented[3] and a standard technique. The loss of lithium can be demonstrated

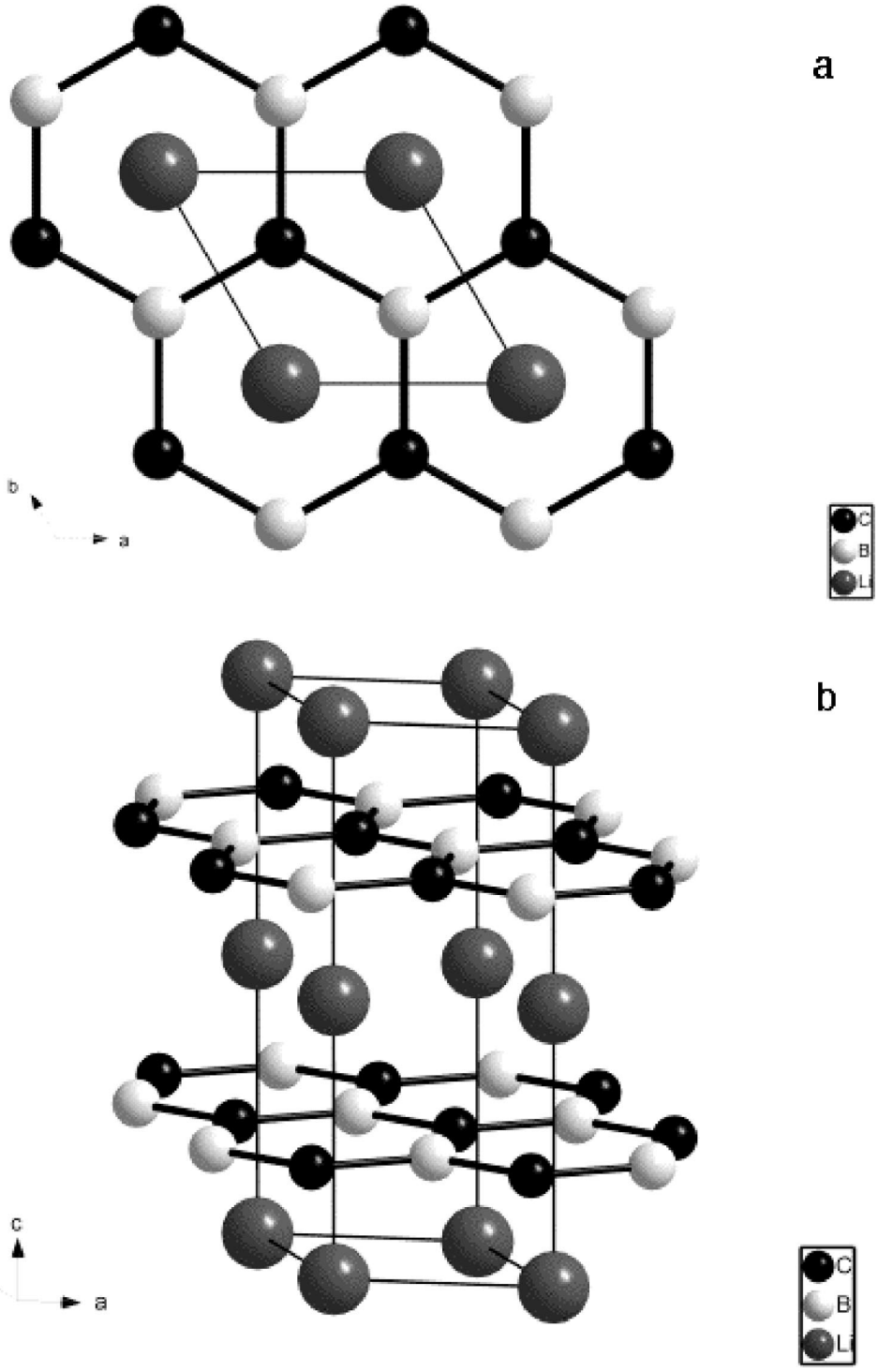

FIG. 1. Crystal structure of LiBC viewed (a) parallel to the stacking direction (b) indicating the B/C alternation due to the layer stacking.

by the placement of an ampoule of TiO_2 further along the furnace tube. During the course of the reaction this turns black as a result of the formation of lithium titanates. The golden polycrystalline sample was handled under an inert atmosphere and characterized by powder x-ray diffraction, SQUID magnetometry, and Raman spectroscopy. Rietveld refinement of the powder data within the GSAS suite gave the lattice constants $a = 2.74857(2)$ Å and $c = 7.0530(2)$ Å in good agreement with the published structure.

B. Deintercalation chemistry

Lithium deintercalation reactions were performed by the reaction of LiBC with an appropriate volume of a 0.22 M solution of $NOBF_4$ in acetonitrile to give the desired reaction stoichiometry under an argon atmosphere. Reactions were performed over a stoichiometry range of 0.25–2 mol $NOBF_4$ per mole of Li. The solutions were heated at 95 °C for 24 h before being allowed to cool and settle. The supernatant solution was then removed and the solid washed with acetoni-

trile before being dried under vacuum. The products typically consisted of red/bronze crystals and were characterized by powder x-ray diffraction, Raman spectroscopy, SQUID magnetometry with the lithium stoichiometry determined by ICP AES on a Spectro Ciros spectrometer following digestion of the samples in aqua regia.

C. Powder x-ray diffraction

Data were collected on a Stoe Stadi-P instrument in transmission geometry with Cu $K\alpha 1$ radiation and a linear position sensitive detector. Samples were sealed under helium in 0.5 mm capillaries and rotated about the capillary axis during data collection to minimize preferred orientation effects. Variable temperature data were collected over the 300–923 K range in a Stoe furnace (high temperature attachment 0.65.1) and analyzed with the Rietveld method using the GSAS software. At higher temperatures decomposition occurred resulting from a reaction between LiBC and the silica capillary. A March-Dollase preferred orientation correction was applied and Li and B/C atoms were refined with separate isotropic displacement parameters.

D. SQUID magnetometry

All measurements were performed on a Quantum Design MPMS-XL SQUID magnetometer. Low-field (field- and zero-field cooled in 40 G) measurements were made to search for superconductivity on deintercalated Li_xBC samples. The temperature dependence of the normal state susceptibility of LiBC was determined by the measurement of magnetization-field isotherms (0–2 T) at eleven temperatures between 5 and 300 K. The sample was contained in a gelatin capsule whose diamagnetic contribution was determined separately in equivalent experiments and subtracted, along with appropriate diamagnetic corrections for the constituent atoms, to afford the paramagnetic normal state susceptibility.

E. Raman spectroscopy

Data were collected on pristine LiBC and deintercalated Li_xBC using a fiber optic probe instrument based upon a Renishaw Compact System 100 spectrometer, with a holographic filter at a low angle of incidence acting as a beam splitter. This has the dual purpose of injecting the illuminating laser light (Ar^+ laser, 514.531 nm) into the optical path, and rejecting scattered light of the laser wavelength of the resulting Raman spectrum. The incident power was approximately 7 mW. The wavelength scale was calibrated against the emission lines of a neon lamp. Spectra were recorded in the backscattered geometry using a $\times 20$ high numerical aperture objective lens, giving a sample area of approximately 100 μm diameter. Data were also collected with a Jobin Yvon Labram 300 with 514.5 nm excitation operating in backscattering geometry and referenced to silicon (520.7 cm^{-1}).

F. Electronic structure calculations

Electronic structure calculations have been performed with both full-potential LAPW (Ref. 7) and pseudopotential codes.[8] The densities of states obtained from these are in excellent agreement with each other and with results in the literature.[4,5] The computationally cheaper pseudopotential codes have been used to determine optimized geometries and to explore the influence of structure on the densities of states. The optimized geometries obtained are identical to the published structures (even when starting from deliberately broken symmetry), albeit with slight differences in the lattice constants. Densities of states obtained for these structures were essentially indistinguishable from those obtained with the published structures, therefore in the following, band-structures and densities of states are shown for materials with the experimentally determined lattice parameters. Although densities of states are comparable, we find that the energy differences between related structures of the same materials (e.g., the difference in total energy for two different lattice constants) depend on the computational methods used. The difference in total energy between two structures is typically 30–60 meV larger in the pseudopotential results than in those from the full-potential codes.

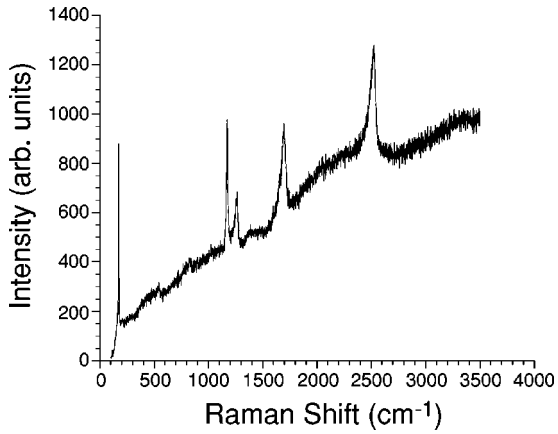

FIG. 2. Raman spectrum of LiBC.

III. RESULTS

X-ray powder diffraction data confirm the formation of pure LiBC by the synthetic procedure described above. The Raman data are shown in Fig. 2. Factor group analysis in D_{6h} predicts $3A_{2u}+2B_{1g}+B_{2u}+3E_{1u}+E_{2u}+2E_{2g}$ modes at the Γ point of the Brillouin zone, with the two E_{2g} modes being Raman active, as in graphite intercalation compounds which share the same layer stacking sequence and space group.[9] In LiBC, these E_{2g} bands are observed at 166 and 1166 cm^{-1}. The major feature at 1166 cm^{-1} is consistent with the higher frequency $E_{2g(2)}$ type graphite mode in which B and C atoms neighboring within the layer move out of phase with each other. This mode is found at 1582 cm^{-1} in graphite, and similar in-plane stretching modes are at 536 cm^{-1} in MgB_2 and 954 cm^{-1} in metallic but nonsuperconducting AlB_2.[10] The absence of the pronounced softening of this mode in LiBC is consistent with the lack of strong electron-phonon coupling. This mode is at a slightly higher frequency than the infrared active 1180 cm^{-1} E_{1u} mode.[6] The extra structure visible in the Raman spectrum of LiBC is

robust, occurring in all preparations, and may arise from the phonon density of states[11] or from the presence of graphite-like defects of sp^3 hybridized carbon. It is comprised of strong bands at 1256, 1688, and 2520 cm^{-1} which are comparable to typical graphite features with the latter corresponding to the second order peak.[12]

The magnetization isotherms measured to determine the normal state susceptibility are shown in Figs. 3(a) and 3(b) and the derived temperature dependence of this quantity is given in Fig. 3(c). The small magnetization of LiBC and the need to correct for ferromagnetic contamination necessitated the measurement protocol used. The ferromagnetic component was removed by saturating in fields of above 1 T and determining the linear susceptibilty at each temperature from the accurately determined (via the number of data points used) high-field magnetization isotherms. The diamagnetic contribution of the sample holder determined at each temperature by the same method was then subtracted. The resulting susceptibility is an upper bound on the intrinsic susceptibility of LiBC due to the possibility of unsaturated contributions from the ferrromagnetic impurities within the fitted field range of 12–20 kG. The magnetization of the ferromagnetic impurity corresponds to 0.001 mol % iron. The 300 K molar susceptibility value of $1.90(7)\times10^{-7}$ emu mol^{-1} is the sum of diamagnetic core and paramagnetic (Pauli and van Vleck) contributions. The diamagnetic correction was made using tabulated values [Li^+: -0.7×10^{-6},[13] (elemental) B: $P6.7\times10^{-6}$,[14] and C (graphite): 6.0×10^{-6} (Ref. 14)] but it should be noted that these will not reflect the influence of the B-C bonding which may be substantial. The resulting 300 K molar susceptibility value of 1.36×10^{-5} emu mol^{-1} reflects both the van Vleck susceptibility due to interband transitions across the $\sim$0.84 eV gap and any Pauli contribution; the upper limit of the density of states at the Fermi level is 0.003 states per eV per LiBC formula unit and will be further reduced from this small value by the van Vleck contribution. The increase in susceptibility below 50 K is equivalent to the Curie-law contribution of 0.2% of localized $S=1/2$ spins. It should, however, be noted that as the measured susceptibility is less than typical values for the diamagnetic correction the calculated density of states is strongly dependent on the actual values used (the values used were conservative in that they gave the lowest value of the Pauli contribution) and the measured value indicates that the Pauli contribution, uncorrected for the Landau diamagnetism and Van Vleck paramagnetism, is comparable in size to the core diamagnetism.

The powder x-ray data at ambient temperature do not show pronounced anisotropic broadening that might be expected from the lamellar nature of LiBC, although even in rotating capillary geometry quantitative Rietveld analysis required the application of a March-Dollase preferred orientation correction along the layer stacking [001] direction. However, two samples displayed visible shoulders on reflections with even *l*. This may be due to phase separation arising from compositional differences or a different stacking sequence, or due to *AA* stacking faults. The *AA* stacking sequence would not contribute to odd *l* reflections. If it is assumed that the extra reflections are due to a second LiBC phase rather than resulting from *AA* stacking faults in the *AB* LiBC structure they can be indexed on a cell with $a=2.7427(12)$ Å and $c=7.0758(36)$ Å. Rietveld refinement of a biphasic model accomodates 16% of a second phase

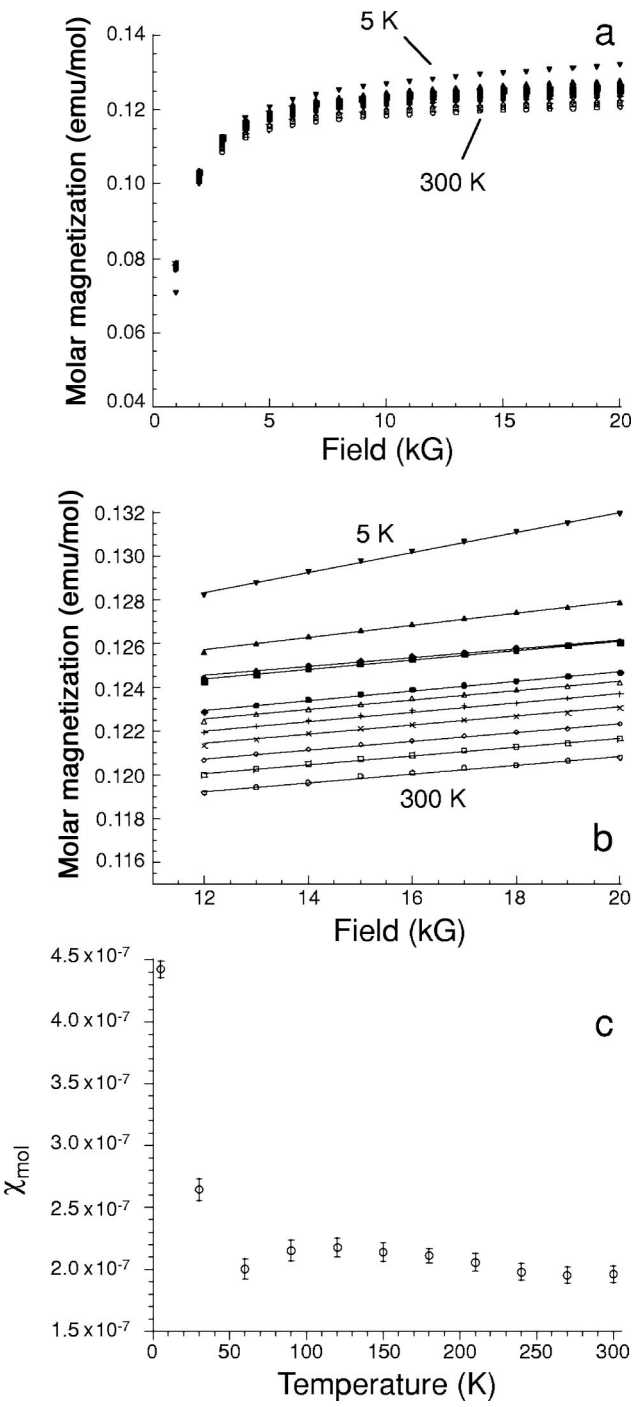

FIG. 3. (a) Molar magnetization versus field as a function of temperature for LiBC from 300 K (bottom) to 5 K (top). (b)Linear fits to the high-field isotherms are used to extract the susceptibility which is corrected for the contribution of the gelatine capsule container. (c) Variation of the molar paramagnetic susceptibility of LiBC with temperature. The data shown have been corrected for the capsule but not the core diamagnetic correction. Calculation of $N(E_f)$ from the above data using the appropriate diamagnetic corrections gives 0.003 states/eV per formula unit at 300 K.

modeled as *AA* stacked, and thus not contributing to the *l* odd reflections [$P\bar{6}m2$ symmetry, $a=2.7436(2)$ Å, $c=3.5315(2)$ Å]. Analysis of the x-ray data in lower symmetry groups such as $P\bar{3}m1$, corrresponding to puckering of the BC layers, was unstable. These observations are significant in the context of the shallow temperature dependence of the conductivity of LiBC and the nonzero density of states at the Fermi level.

The temperature dependence of the diffraction data and the extracted cell metrics is shown in Fig. 4. The linear thermal expansion parameters α_c and α_a in the interlayer and intralayer directions, respectively, were derived from the temperature dependence of the associated cell parameters according to Eq. (1)

$$\alpha=\frac{(\Delta l/\Delta T)}{l_0}. \tag{1}$$

The derived values near room temperature are $\alpha_a=5.59(6)\times10^{-6}$ K^{-1} and $\alpha_c=2.83(10)\times10^{-5}$ K^{-1}, compared with $\alpha_a=5.4\times10^{-6}$ K^{-1} and $\alpha_c=1.14\times10^{-5}$ K^{-1} near room temperature for MgB_2.[15] MgB_2 itself is unusual in the anisotropy of these values with only VB_2 having a larger $\alpha_c=1.4\times10^{-5}$ K^{-1} in the binary metal diborides.[16] Thus while the in-plane thermal expansion of LiBC determined in the present measurements is consistent with similar in-plane bonding to MgB_2 and the lamellar metal diborides, the out-of-plane expansion is quite extraordinary. This suggests that the interlayer bonding is particularly weak in LiBC, suggesting that the interlayer covalent interactions between Li and B/C are weaker even than those between Mg and B in MgB_2. Total energy calculations discussed below do not, in fact, show any significant difference in the behaviors of MgB_2 and LiBC expanded along the *c* axis. However, the very modest thermal expansions result in energy costs of only ~10 meV in both cases, and any differences on such small numbers are insignificant in comparison to the errors in density functional methods. There is a pronounced dependence of the electronic properties on the stacking of the BC sheets in LiBC, which may make this observed difference in the bonding anisotropy compared with metallic and superconducting MgB_2 particularly important. That the interlayer expansion is dominated by metal-boride covalency can be seen from the much larger α_c value of 5.9×10^{-5} K^{-1} determined for the first stage graphite intercalation compound LiC_6.

The thermal expansion data can be modeled with an Einstein equation using a single phonon energy

$$\ln\frac{a}{a_0}=\frac{A\theta}{e^{\theta/T}-1}, \tag{2}$$

where *a* is the metric parameter (*a*, *c*, or *V*), a_0 its value at $T=0$ K, θ is the phonon energy, *T* is the temperature, and *A* is a scaling coefficient. The fits shown in Figs. 4 and 5 are to Eq. (2). Although the data do not extend low enough in temperature for a reliable determination of the phonon energy, the values of 1284 (314) K (*a*), 1007 (120) K (*c*), and 1084 (167) K (*V*) are all approximately double the values found for MgB_2.[15] This is qualitatively consistent with the higher in-plane stretching frequencies seen in Raman and infrared measurements, and with the absence of phonon softening due to the electron-phonon coupling implicated in the superconducting pairing mechanism in MgB_2. The phonon frequencies and thermal expansion parameters both make clear that although MgB_2 and LiBC are formally isoelectronic, the details of the strength and isotropy of the bonding in the two materials are quite different.

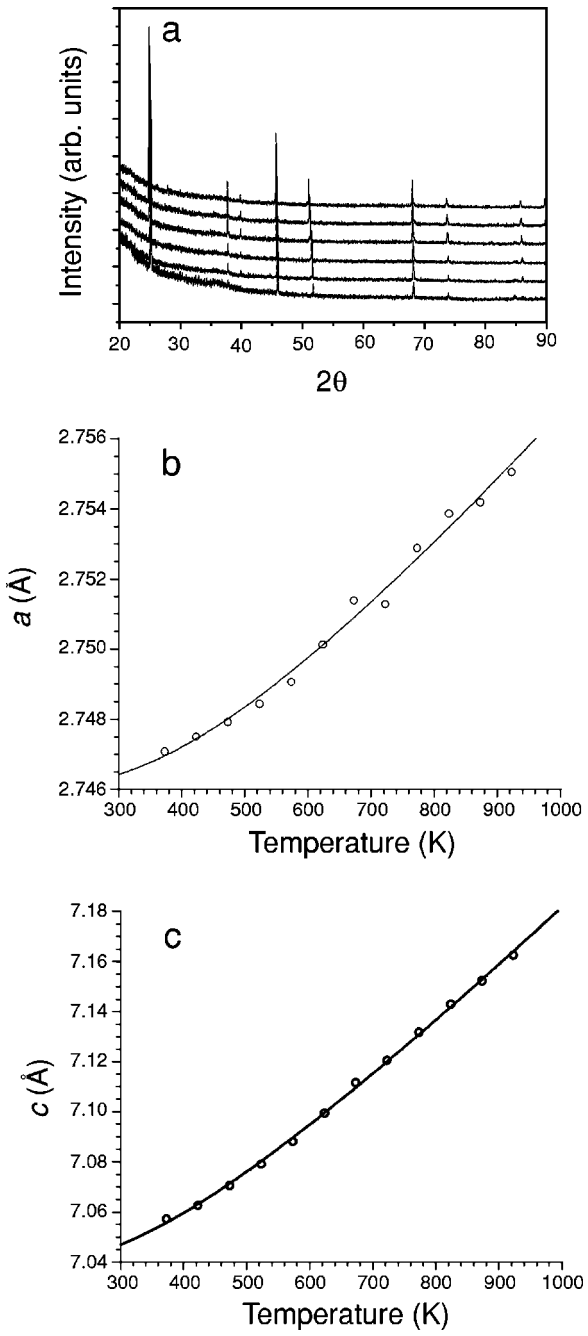

FIG. 4. (a)Variable temperature powder x-ray diffraction data from LiBC. The data sets from top to bottom correspond to collection at 600, 500, 400, 300, 200, 100 °C. (b) Variation of *a* with temperature. Data are fitted to the Einstein equation (2) with the parameters discussed in the text. (c) Variation of *c* with temperature, with fit as in (b).

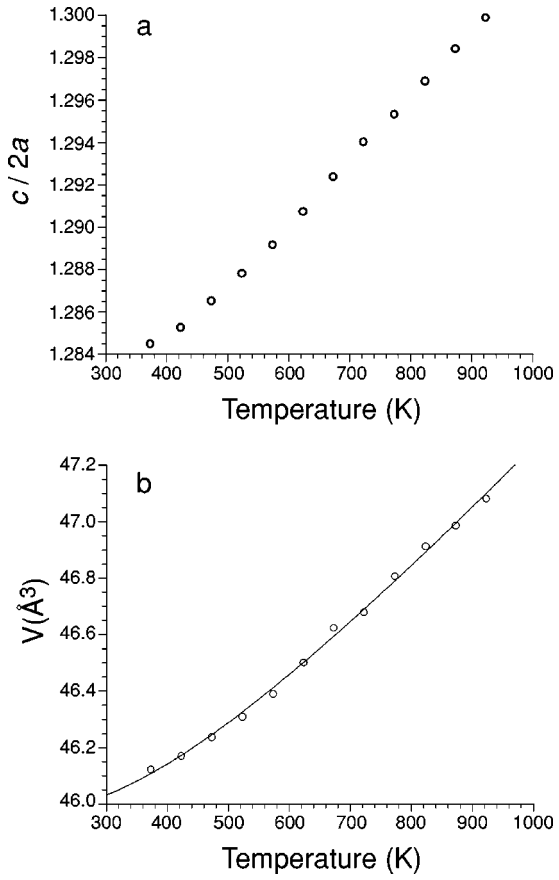

FIG. 5. (a) Variation of c/2a with temperature. (b) Variation of the unit cell volume of LiBC with temperature. The data are fitted as in Fig. 4(b).

Chemical oxidation of layered intercalation compounds at low temperature is an important and very well studied area, with the alkali metal intercalation compounds of graphite displaying extensive examples of such chemistry. The bonding in MgB_2 and the layered diborides is sufficiently three dimensional that the layered intercalate bonding well suited to describing graphite intercalation compounds with their much reduced interlayer covalency is not useful. The introduction of carbon, with its enhanced electronegativity, into the layers of LiBC offers the opportunity to investigate chemistry analogous to that of graphite. Thermal deintercalation to afford $Li_{0.24}BC$ without significant variation of the unit cell parameters was reported in the original paper on the discovery of LiBC.[3] We have used the powerful oxidizing agent $NO^+BF_4^-$ in acetonitrile at 95 °C to remove Li in a controlled manner from LiBC. This is possible up to a limiting value of $Li_{0.5}BC$ according to chemical analysis of both the supernatant solution and the oxidized solid. X-ray powder diffraction data indicate (Fig. 6) that the infinite hexagonal layer structure of LiBC is maintained with unchanged cell parameters for Li_xBC samples with $x=0.5$ and 0.65. Low-field SQUID magnetization data demonstrate that these solids are not superconducting. The reason for this becomes apparent when the Raman spectra (Fig. 7) of these materials are considered. It is clear that the phonon features associated with the LiBC structure disappear systematically as the oxidation level increases, with the remaining features being consistent with highly disordered amorphous graphite.[17] The absence of any LiBC features in the Raman despite the persistence of well-defined and highly crystalline LiBC reflections in the x-ray powder diffraction patterns suggests that the Raman data probe the surface of the Li_xBC system to a greater extent than the Cu $K\alpha$ x-rays, which will penetrate the sample completely. The data therefore suggest that oxidation produces a disordered graphitelike BC material which coexists with largely unreacted LiBC, thus accounting for the absence of electronic behavior predicted theoretically for

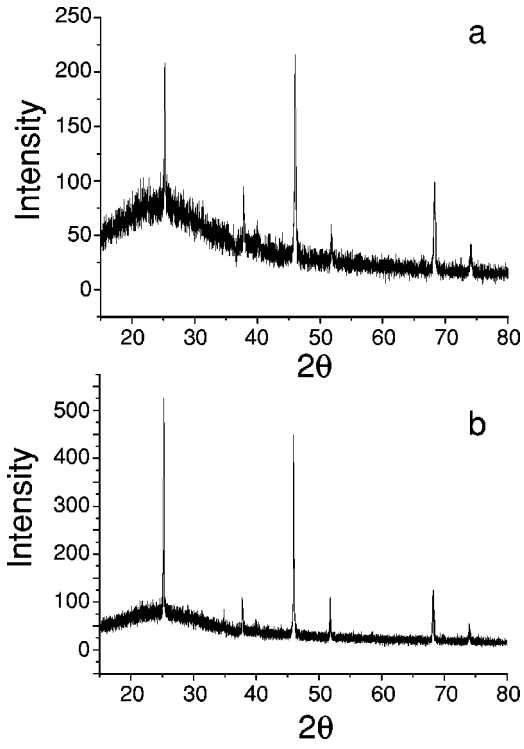

FIG. 6. Powder x-ray diffraction data from Li_xBC (a) $x=0.5$ (b) $x=0.65$. The crystallinity decreases as more $NOBF_4$ is used in the deintercalation reaction.

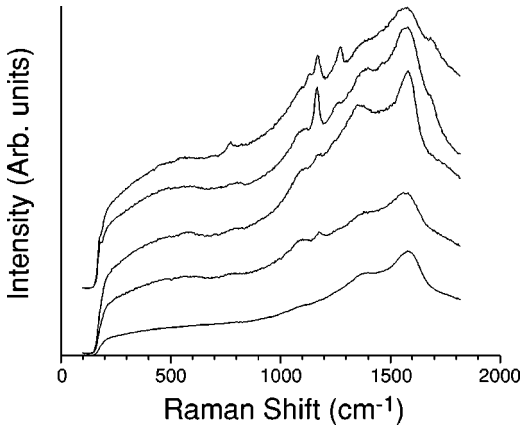

FIG. 7. Raman spectra of Li_xBC multiphase assemblages. The spectra are (top to bottom): LiBC + 0.25 $NOBF_4$ ($Li_{0.9}BC$), LiBC + 0.5 $NOBF_4$ ($Li_{0.85}BC$), LiBC + 0.75 $NOBF_4$ ($Li_{0.77}BC$), LiBC + 1.0 $NOBF_4$ ($Li_{0.72}BC$), LiBC + 2.0 $NOBF_4$ ($Li_{0.62}BC$).

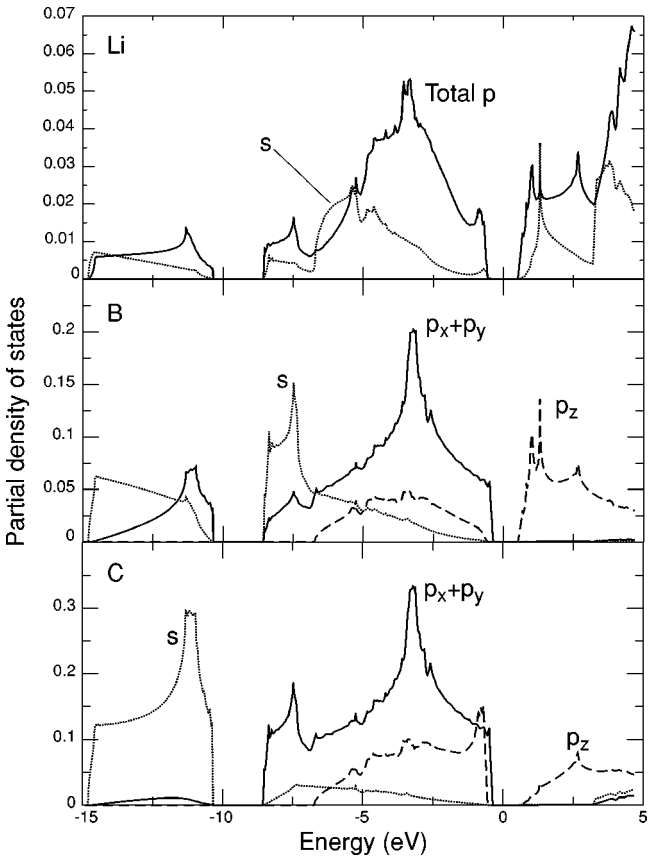

FIG. 8. Density of states projected onto atomic orbitals in LiBC, computed with a full-potential LAPW method with 546 *k* points in the irreducible wedge of the Brillouin zone. The Fermi energy has been aligned with the center of the bandgap. The experimentally determined structure and lattice parameters were used.

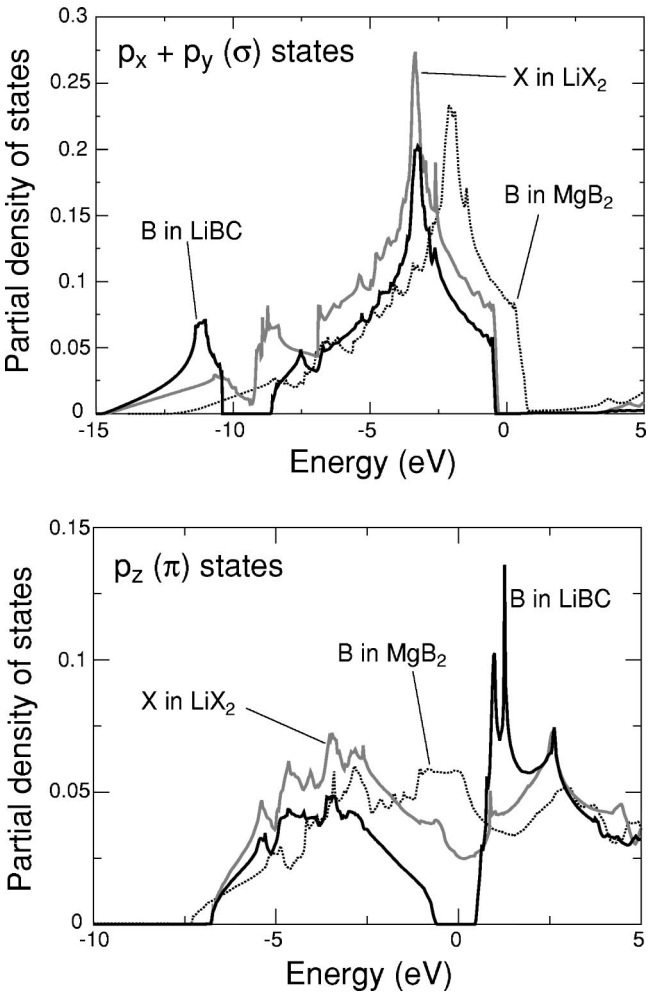

FIG. 9. Partial densities of states on B atoms in LiBC compared to that on the B atoms in MgB_2 and in the *X* atom (with atomic number 5.5) in the model compound LiX_2. The bandgaps in the σ and π states of LiBC can be seen to arise from the symmetric alternation of the B and C atoms both within the planes and between planes. For LiBC, the published structures and lattice parameters were used, while for the model compound, the MgB_2 structure was used, but with lattice parameters chosen to match those of LiBC.

Li_xBC systems. The synthetic difficulties in preparing such materials should not therefore be underestimated. The detailed chemical description of the disordered BC phase is of interest as B doping of graphite is difficult to achieve at this level. The asymptotic limit of *x* under those low-temperature deintercalation conditions appears to be 0.5, suggesting that this is a kinetic limit due to the microstructure of the oxidized biphasic material thus formed, and consistent with the larger extent of deintercalation accomplished thermally in the previous report. It is clear that x-ray powder diffraction alone is insufficient to study the deintercalation chemistry of these materials.

In MgB_2, the superconductivity is determined by the σ in-plane B-B bonding states. Straddling the Fermi energy, these couple strongly with the in-plane B-B vibrations. The bonding has been described in terms of the competing filling of the σ states and of the out-of-plane π states.[2] Interaction with the Mg ions pulls the π states below E_f and they are occupied at the expense of σ states pushed above E_f. LiBC is isoelectronic with MgB_2, and has very similar bonding, dominated by σ states in the BC layer. The partial density of these states is remarkably similar to the partial density of σ states in MgB_2. However, as can be seen in Fig. 8, the σ states are fully occupied in LiBC, with the band edge lying 0.5 eV below E_f. Additionally, there is a gap in the σ states from 10.4 to 8.6 eV. The p_z-derived π states are located on either side of E_f. LiBC in the published structure is thus formally an insulator, as there is a gap in the π states at E_f.

Several effects contribute to these electronic properties. The energetic regions in which the states occur is determined largely by the atomic potentials, while the band gaps open as a result of symmetry. This becomes clearer if we compute the electronic structure for LiX_2, where *X* has a nuclear charge $Z=5.5$, i.e., it is "an average" of the B and C atoms, and the material has an MgB_2 structure with lattice parameters appropriate to LiBC. It can be seen in Fig. 9 that the gaps in the bands of LiBC are absent in the electronic structure of the higher symmetry, model material. The model has essentially the same bandstructure as MgB_2, but with the Fermi energy above the B-C σ bands, as shown by Rosner *et al.*[4] Although the band gaps are absent, the densities of

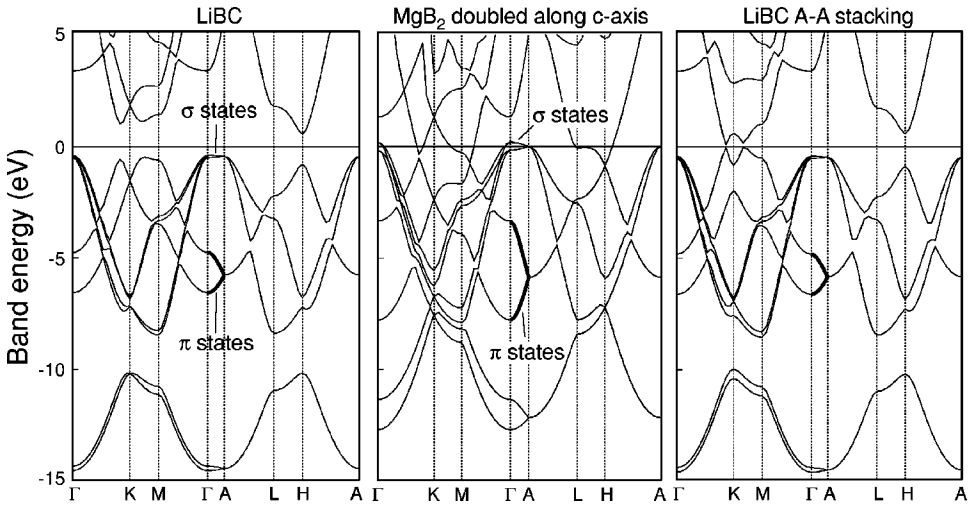

FIG. 10. Bandstructures of LiBC, MgB_2, and the putative *A*-*A* stacking of LiBC, with alternation of the B-C within the plane, but not between planes. For more direct comparison, the structure has been repeated along the *c* axis for both MgB_2 and LiBC *A*-*A* stacking to give *c* axes similar to LiBC. This causes a folding back of the bands from the *A* point in the center of the plot. Published structures have been used for LiBC and MgB_2, while the lattice parameters of LiBC were used for the *A*-*A* stacked material (densities of states for the geometry optimized structure are essentially identical).

states are otherwise identical to those of LiBC, with σ and π bands spanning the same energy range in both materials. The gaps in the LiBC bands then clearly result from symmetry, i.e., from the alternation of B and C atoms, both within the plane, giving rise to the gap in the σ band, and between adjacent planes, giving rise to the gap in the π states, as there are no corresponding gaps in the electronic structure of the averaged (or infinitely disordered) material.

From the suggested model of bonding in MgB_2 (Ref. 2) it might have been thought that occupation of the π states would lead to an upshift and depopulation of the σ states in LiBC, however, this is clearly not the case. In LiX_2 the occupation of the π states is comparable to that in MgB_2, but the σ bands occur in the same energy range as those of LiBC. In particular, the band edge occurs at the same energy (if the Fermi energy of the insulator LiBC is located in the center of the gap in the π bands) as does the main peak in the pDOS. There is, however, a much smaller covalent interaction between the Li and the BC layer than between the Mg and the B layer: the orbital overlap population for Mg-B bonds is -2.13, whereas for Li-B it is only -0.12, and for Li-C even smaller at -0.03. For MgB_2 electron transfer and electrostatics alone do not lead to upshift and depopulation of the σ states, the covalent Mg-B interaction is vital. In LiBC the reduction in this covalent interaction makes the p_z states at E_f fairly localized and largely B or C p_z orbital in character. Thus, the σ states are located at lower energy in LiBC than in MgB_2 because of the more attractive potential of the C atom and because of substantially smaller covalent interaction of the metal with the *p*-block elements in the layer, i.e., LiBC would be insulating in the plane even if B and C did not alternate in the planes.

The experimental observation of nonzero density of states at the Fermi level and semimetallic conductivity contrasts strongly with the ~ 1 eV band gap predicted by band structure calculations both here and in the literature[4,5] for the perfect LiBC structure. However, as shown in Fig. 9, the gap at E_f arises from the alternation of B and C atoms along the *c* axis. LiBC in a structure with an *A*-*A* stacking sequence (with each atom type occupying identical sites in all layers) has σ bands essentially identical to those of LiBC in the *A*-*B* stacking sequence, but a p_z projected DOS very similar to the model compound LiX_2. This can also be seen in the bandstructure plots in Fig. 10. Over most of the Brillouin zone the bands of the *A*-*A* material are perfectly superposable on those in the *A*-*B* stacking sequence, except in the region of the *K* point, where a slightly greater dispersion of the B-C p_z states pushes them across the Fermi energy. The *A*-*A* stacking sequence is only slightly higher in energy than the ground-state *A*-*B* sequence, we obtain a difference of 45 meV (65 meV with the pseudopotential methods). It is important to note that this energy difference is much smaller than thermal energies at the synthesis temperature. The x-ray diffraction data suggest that in some samples, there is evidence of a smaller *c* axis. This may possibly arise from the alternative stacking, perhaps present as stacking faults. We have explored how stacking faults affect the electronic structure. There is a steady increase in the density of states at E_f as the density of *A*-*A* stacking faults increases, however at the lowest density examined (20%) there are fewer than 10^{-3} states per eV per spin at E_j. Li vacancies may also contribute to the density of states at E_f by hole doping of the σ bands, although none were detectable at the sensitivity limits of x-ray power diffraction.

A final possible contribution to the density of states at E_f could come from puckering of the B-C layers, as suggested by Hlinka *et al.* [11] Reducing the symmetry of the LiBC structure to $P\bar{3}m1$ by buckling the layers by ± 0.2 Å [similar to the buckling in MgB_2C_2 (Ref. 18)] results in a much larger density of states, 0.15 states/eV per formula unit per spin, at E_f. However, this puckering of the layers agrees with nei-

ther the x-ray data nor the density functional calculations for LiBC. The puckered structure is not at a minimum of energy, and geometry optimization relaxes the atom positions back to the standard LiBC structure. If the BC layers are puckered by ± 0.2 Å, the energy is increased by ~ 1.2 eV per formula unit (as determined using the pseudopotential methods) relative to the published structure, while a puckering of ± 0.1 Å increases the energy by 0.37 eV. This should be contrasted with the much smaller 0.065 eV per formula unit required to change the stacking from *A*-*B* to *A*-*A*. More generally, both the stacking fault and plane buckling motifs for suppressing insulating behavior should be borne in mind in synthetic chemistry focusing on inducing metallic behavior in doped LiBC derivatives or their relatives.

The density functional calculations shed little light on the difference in thermal expansion between MgB_2 and LiBC. Indeed if the MgB_2 structural unit is repeated along the *c* axis to give unit cell dimensions and contents consistent with LiBC, then the band structures can be seen to be remarkably similar, as shown in Fig. 10. Focusing on the Γ-*A* direction, which gives the dispersion along the *c* direction, the slight shifts in energy of the very flat σ bands can be seen to move them below E_f in LiBC and in the putative *AA* stacked polymorph. The bands in the region of -5 eV (shown in bold) are derived from the π-states in the B-C layer, and these clearly disperse to a greater extent in MgB_2 than in LiBC, i.e., the states responsible for interplanar bonding appear more localized in LiBC, because of the greater localization of the carbon p_z states and the much smaller contribution of the metallic states to the bonding (as evidenced by the near zero orbital overlap). This difference in interaction between the layers can be seen clearly in Fig. 11, which shows plots of the wave function of the state at the bottom of the band highlighted in the Γ-*A* direction in Fig. 10. The π character of this state is evident, as in the bonding between layers. For LiBC, the Li atom is involved in the bonding to a negligible extent, whereas the intensity is much greater on the Mg atom in MgB_2. The alternation of the B and C in the *c* direction of LiBC is a contributory factor to the weaker bonding, although even for the *A*-*A* stacking, the C p_z state is too localized for significant interplanar bonding, which is only weakly evident for the B p_z state. For MgB_2, the B p_z states interact much more strongly between planes. This may explain the difference in thermal expansion along *c*, however there is no evidence of this in the total energies, which change by the same amount for the same change in interplanar spacing in LiBC and MgB_2, within the errors in the calculations.

Smaller interplanar Coulomb attraction may also contribute to the difference in stretching along the *c* axis. For MgB_2, Mulliken analysis gives the charges as Mg $+1.83e$ and B $-0.92e$, whereas for LiBC, there is one fewer electron for the metal to contribute (the other coming from the C atom) giving charges on the Li of $+0.93e$, and on the B of $-0.23e$ and C of $-0.7e$ (there is a marked difference in charges on the B and C atoms). As it contains fewer electrons, the Li layer should also be less able to provide screening of the Coulomb repulsion between the B-C layers. Once again, however, these differences do not seem to translate into noticeable differences in the total energies for expansion of the *c* axis of these materials. The small energy differences for the relatively small thermal expansions (~ 10 meV for expansion by 0.1 Å) are likely too small to be reliably compared between the two materials.

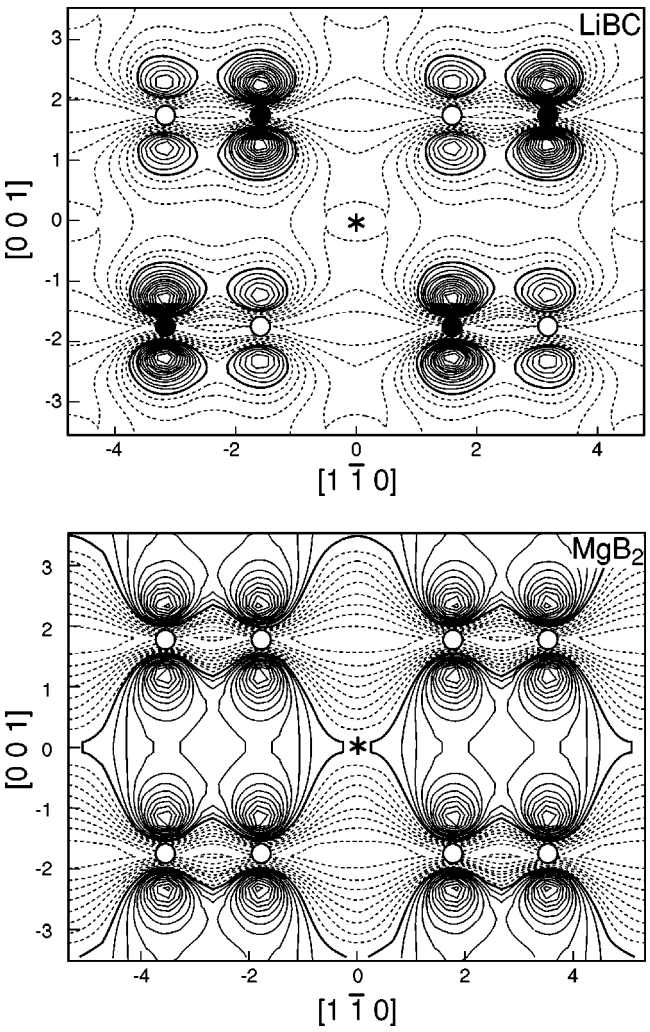

FIG. 11. Contour plots of the orbital at the bottom of the π band highlighted in Fig. 8. Contours values range from 0.00535 to 0.18772 in steps of 0.01013 for LiBC and from 0.0051 to 0.17468 in steps of 0.00892 for MgB_2. Contours below 0.076 are shown dashed. There is a much stronger interplanar interaction in MgB_2 mediated by the B p_z states than in LiBC, where the C p_z state is more strongly bound and localized and there is little B p_z C p_z interaction along the interlayer direction.

IV. CONCLUSIONS

Band structure calculations on the perfect LiBC structure reveal wide band-gap behavior. This is not consistent with recent conductivity measurements. However, the pronounced influence of the stacking sequence of the BC layers on whether the material is metallic or insulating indicates the powerful effect defects, such as faults in the stacking sequence, could play in controlling the electronic properties. The small upper limit of any Pauli paramagnetic contribution

to the susceptibility is consistent with only very subtle deviations from the perfect structure. B/C disorder within the hexagonal layers also induces metallic behavior in model calculations, although it should be noted that the associated disorder potentials may induce Anderson localization. The interlayer bonding appears weaker in LiBC than in MgB_2 as demonstrated by the remarkable *c* axis linear thermal expansion, whereas the in-plane phonon frequencies are considerably higher due to the absence of softening induced by electron-phonon coupling.

Electronic structure calculations show LiBC to be remarkably similar to MgB_2, differing most importantly in the energy of the σ states in the B-C planes which lie ~ 0.5 eV below E_f, whereas in MgB_2 the σ states in the B-B planes straddle E_f. This difference arises because of weaker bonding with the metal and from the greater electronegativity of the carbon atoms, which produces a pronounced charge separation on the nodes of the decorated graphite sheet. The symmetry of the B-C layers, alternating B and C atoms in the hexagonal ring, induces a bandgap in the σ states, while the alternation in B and C between planes induces a band gap at E_f in the π states. In the alternative *A*-*A* stacking sequence, the gap in the π states at E_f disappears, but the occupation of these states does not affect the σ states. The small energy cost of inducing the *A*-*A* stacking suggests that stacking faults may contribute to the density of states at E_f; however, buckling of the B-C layers is ruled out by both the x-ray diffraction and density functional results. It is possible to deintercalate lithium from the structure using low-temperature soft chemistry methodology, but this produces an inhomogeneous biphasic material with surface layers rich in material whose vibrational properties are similar to amorphous graphite. Subsequent treatment of this material may afford crystalline Li_xBC and is an important future task. The metal boron covalency therefore makes the intercalation chemistry of these materials quite different from that of graphite.

ACKNOWLEDGMENTS

We thank EPSRC for funding under Grant Nos. GR/R53999 and GR/R47936.

[1] J. Nagamatsu, N. Nakagawa, T. Muranaka, Y. Zenitani, and J. Akimitsu, Nature (London) **410**, 63 (2001).
[2] J. M. An and W. E. Pickett, Phys. Rev. Lett. **86**, 4366 (2001).
[3] M. Wörle, R. Nesper, G. Mair, M. Schwarz, and H. G. von Schnering, Z. Anorg. Allg. Chem. **621**, 1153 (1995).
[4] H. Rosner, A. Kitaigorodsky, and W. E. Pickett, Phys. Rev. Lett. **88**, 127001 (2002).
[5] P. Ravindran, P. Vajeeston, R. Vidya, A. Kjekshus, and H. Fjellvag, Phys. Rev. B **64**, 224509 (2001).
[6] A. V. Pronin, K. Pucher, P. Lunkenheimer, A. Krimmel, and A. Loidl, cond-mat/0207299 (unpublished).
[7] K. Schwarz, P. Blaha, and G. K. H. Madsen, Comput. Phys. Commun. **147**, 71 (2001).
[8] V. Milman, B. Winkler, and J. A. White, Int. J. Quantum Chem. **77**, 895 (2000).
[9] G. L. Doll, P. C. Eklund, and J. E. Fischer, Phys. Rev. B **36**, 4940 (1987).
[10] B. Renker, K. B. Bohnen, R. Heid, D. Ernst, H. Schober, M. Koza, P. Adelmann, P. Schweiss, and T. Wolf, Phys. Rev. Lett. **88**, 067001 (2002).
[11] J. Hlinka, I. Gregora, J. Pokorny, A. V. Pronin, and A. Loidl, Phys. Rev. B **67**, 020504 (2003).
[12] D. S. Knight and W. B. White, J. Mater. Res. **4**, 385 (1989).
[13] A. H. Morrish, *Physical Principles of Magnetism* (Wiley, New York, 1965).
[14] *CRC Handbook*, 74th ed., edited by D. R. Lido (CRC Press, Boca Raton, 1993).
[15] J. D. Jorgensen, D. G. Hinks, and S. Short, Phys. Rev. B **63**, 224522 (2001).
[16] B. Lonnberg, J. Less-Common Met. **141**, 145 (1988).
[17] A. C. Ferrari and J. Robertson, Phys. Rev. B **63**, 121405(R) (2001).
[18] M. Wörle and R. Nesper, J. Alloys Compd. **216**, 75 (1994).